ACS APPLIED MATERIALS & INTERFACES

Research Article

www.acsami.org

A Significant Improvement in the Electrocatalytic Stability of N-Doped Graphene Nanosheets Used as a Counter Electrode for $[Co(bpy)_3]^{3+/2+}$ Based Porphyrin-Sensitized Solar Cells

Peng Zhai,[†] Chih-Chi Lee,[‡] Ya-Huei Chang,[†] Chang Liu,[†] Tzu-Chien Wei,*[,‡] and Shien-Ping Feng*[,†]

[†]Department of Mechanical Engineering, The University of Hong Kong, Pokfulam 852, Hong Kong

[‡]Department of Chemical Engineering, National Tsing-Hua University, Hsinchu 300, Taiwan

Supporting Information

ABSTRACT: A significant improvement in efficiency is achieved for porphyrin (YD2-o-C8) based dye-sensitized solar cells, coupled with $[Co(bpy)_3]^{3+/2+}$ mediator electrolyte. However, the poison of the counter electrode (CE) by the $[Co(bpy)_3]^{3+/2+}$ mediator remains a significant barrier to producing a reliable high-performance device. In this paper, nitrogen-doped graphene nanosheets (NG) are produced using a low-cost solution-based process and are used as the CE for $[Co(bpy)_3]^{3+/2+}$ based porphyrin-sensitized solar cells. These produce significantly better electrocatalytic activity than the commonly used Pt CE. The superior performance is a result of the increased number of catalytic sites and the wettable surface that is caused by the substitution of pyridinic and pyrrolic N into the carbon-conjugated lattice. To the authors' best knowledge, the significantly improved cycling stability (>1000 times) of NG CE for $[Co(bpy)_3]^{3+/2+}$ redox complexes is demonstrated for the first time.

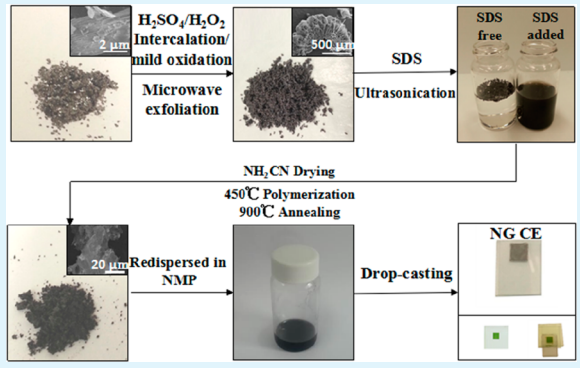

KEYWORDS: *N-doped graphene, cobalt mediator, porphyrin-sensitized solar cells, electrocatalytic reliability, surface wettability*

1. INTRODUCTION

Dye-sensitized solar cells (DSSCs) have been the subject of much study in recent years because they are cost-effective in converting solar energy to electricity.[1] A typical DSSC consists of a dye-sensitized TiO_2 photoanode, an I_3^-/I^- electrolyte, and a Pt counter electrode (CE). The current ruthenium dye in conjunction with an I_3^-/I^- redox couple has been particularly successful because it has slow recombination kinetics, which leads to long electron lifetimes.[2,3] However, the two-electron redox mediator of I_3^-/I^- limits the accessible open-circuit voltage (V_{oc}) to 0.7−0.8 V because there is an excessive voltage loss during the dye-regeneration reaction. Over the past few years, a significant improvement has been made by using zinc porphyrin sensitizers (YD2-o-C8), coupled with a single-electron redox mediator of $[Co(bpy)_3]^{3+/2+}$ electrolyte.[4] Unlike I_3^-/I^- based electrolyte (0.35 V vs NHE), $[Co(bpy)_3]^{3+/2+}$ redox complexes do not require an intermediary step during dye regeneration, and their high redox potential (0.56 V vs NHE) results in an increase in V_{oc} to 0.8−0.9 V.[5,6] Donor-pi-acceptor YD2-o-C8 sensitizers not only absorb light over the whole visible range but also have long-chain alkoxy groups that inhibit the faster interfacial back electron transfer reaction of $[Co(bpy)_3]^{3+/2+}$ redox complexes. Because of this unique combination of YD2-o-C8 and $[Co(bpy)_3]^{3+/2+}$, porphyrin-sensitized solar cells (PSSCs) have achieved a world record efficiency of 12.3% under 1 sun illumination. As PSSCs are still in the infant stage, the long-term stability of PSSCs has not yet been properly investigated. It is important to ensure that $[Co(bpy)_3]^{3+/2+}$ complexes do not undergo irreversible changes at the CE, and it is important to give a stability that is similar to that of I_3^-/I^- electrolyte. Pt is widely used as a catalyst in DSSCs CE,[7] but there is a severe poisoning effect in Co-mediated PSSCs under prolonged potential cycling.[8−10] The poisoning is probably caused by the ligand separating from the $[Co(bpy)_3]^{3+/2+}$ redox complexes. Recently, it has been reported that a graphene-based CE is superior to a Pt CE, both in terms of charge-transfer resistance (R_{ct}) and electrochemical stability, for a $[Co(bpy)_3]^{3+/2+}$ based electrolyte.[11−13] Therefore, PSSCs with graphene-based CEs outperform those with Pt CEs, in terms of fill factor (FF) and power conversion efficiency (PCE).

Until now, only a few studies have reported on the cycling stability of carbon-based CEs in conjunction with $[Co(bpy)_3]^{3+/2+}$ complexes, and the measurements are only for tens of potential cycles. Recently, the use of nitrogen in carbon nanomaterials has been demonstrated to modulate the electronic structures and to further enhance the electrochemical catalytic activity in supercapacitors and DSSCs,[14,15] but very little studies of PSSCs have been conducted. In this paper, nitrogen-doped graphene nanosheets (NG) were prepared

Received: November 27, 2014
Accepted: December 31, 2014
Published: December 31, 2014

DOI: 10.1021/am5083705
ACS Appl. Mater. Interfaces 2015, 7, 2116−2123

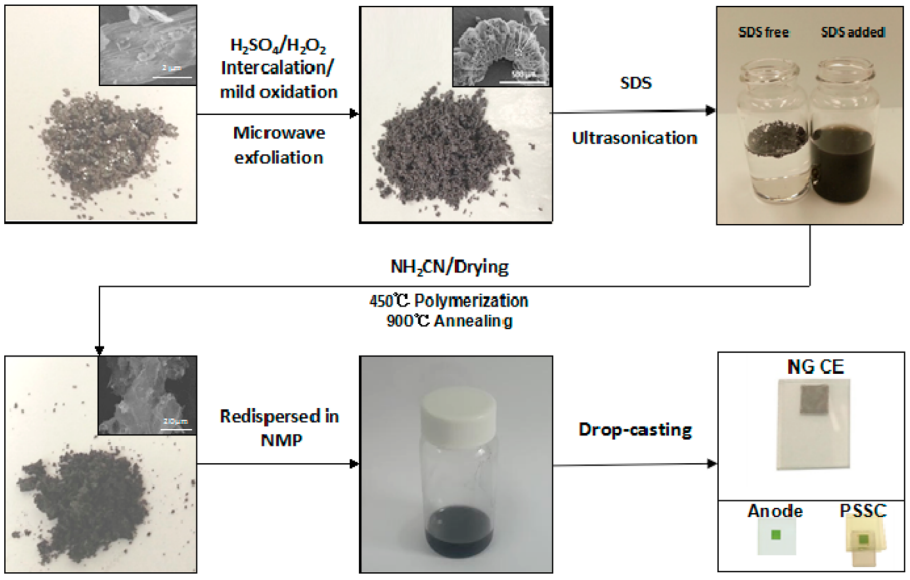

Figure 1. A schematic illustration of the fabrication of NG nanosheets. The natural graphite flakes are intercalated using mildly oxidizing (H_2SO_4/H_2O_2), without further reduction. After rapid microwave irradiation, the expanded graphene nanosheets are well-dispersed in deionized water with SDS under ultrasonication. A nitrogen source is introduced by mixing with a cyanamide solution, followed by polymerization at 450 °C and Ar annealing at 900 °C to synthesize nitrogen-doped graphene. The NG counter electrode is prepared by drop-casting on FTO glass, followed by annealing (500 °C for 1 h).

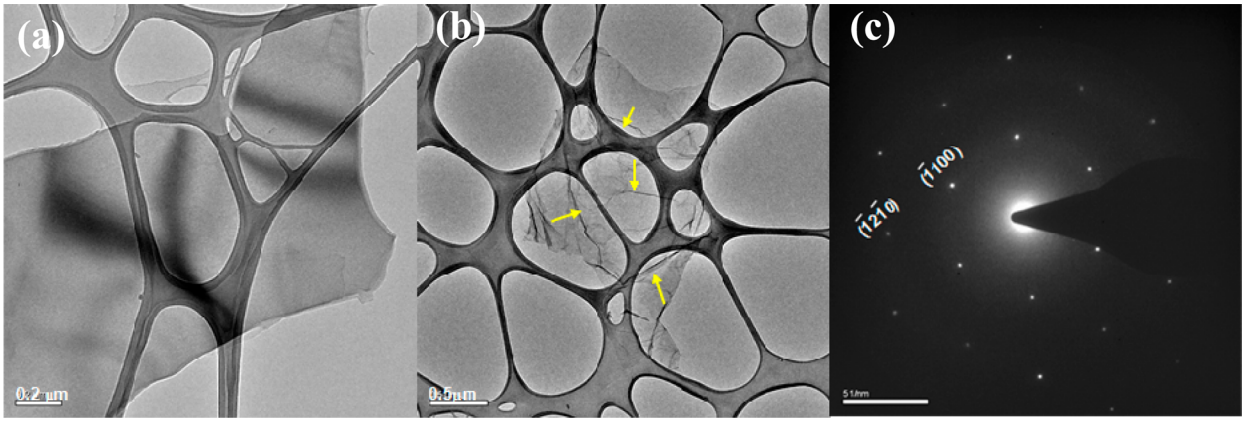

Figure 2. TEM images of (a) flaky graphene nanosheet and (b) curved NG; the yellow arrows show the obvious wrinkle. (c) The corresponding SAED.

using the low-cost solution-based method and were evaluated as CEs in PSSCs. The electrocatalytic activity and surface wettability of NG coated on fluorine-doped conductive glass (FTO) for $[Co(bpy)_3]^{3+/2+}$ redox complexes was determined using electrochemical impedance spectroscopy (EIS), contact angle measurement, and a high-speed video camera. The PCE of a PSSC with an optimized NG CE is 8.30%, but this value for a PSSC with a Pt CE is 7.95%. The significantly improved cycling stability (>1000 times) of an NG CE for $[Co(bpy)_3]^{3+/2+}$ redox complexes is demonstrated for the first time.

2. EXPERIMENTAL SECTION

2.1. Fabrication of Nitrogen-Doped Graphene Nanosheets (NGs). Forty-five milliliters of concentrated H_2SO_4 (96%, Sigma-Aldrich) and 5 mL of H_2O_2 (30%, Prolabo) were mixed as a mild oxidizer. One gram of natural graphite flakes (Sigma-Aldrich) was added into a 50 mL H_2SO_4/H_2O_2 mixture and then was stirred for 120 min at room temperature. The powders were rinsed several times with DI water until the pH value was approximately 7. After filtering and drying, the acid-intercalated graphite flakes were irradiated in a microwave oven (750 W) for 60 s to produce exfoliated graphite flakes. The as-made exfoliated graphite flakes of 0.3 mg/mL and sodium dodecyl sulfonate (SDS, Fluka) at a concentration of 5 mg/mL were added into 30 mL DI water, followed by probe sonication (750 W) for 2 h, to fragment the exfoliated graphite flakes into the graphene nanosheets. Two milliliters of 50% cyanamide (NH_2CN) was then added into a 30 mL graphene-nanosheet suspension, and the mixture was stirred for 12 h. After drying at 90 °C for 12 h, NG powders were obtained via two-step annealing in a tube furnace, involving polymerization at 450 °C for 60 min and Ar annealing at 900 °C for 120 min. The NG powders were redispersed in NMP using ultrasonication (0.5 h, 750 W). The concentration of the NG suspension was about 0.5 mg/mL.

2.2. Fabrication of NG and Pt CEs and EIS Measurement. A Pt CE was prepared by deposition of ca. 30 μL/cm^2 of H_2PtCl_6 solution and was sintered at 400 °C for 15 min. The NG CEs were prepared by drop-casting the NG suspension of 10 μL (NG1), 20 μL (NG2), and 40 μL (NG3) onto FTO glass with an exposed area of 0.36 cm^2, followed by annealing at 500 °C for 1 h in a furnace. The EIS was measured by scanning the symmetric dummy cell (CE/electrolyte/CE) using a potentiostat (CHI 660E), from 100 kHz to 0.1

DOI: 10.1021/am5083705
ACS Appl. Mater. Interfaces 2015, 7, 2116−2123

Hz, with 5 mV amplitude in the open-circuit condition. The catalytic stability test was performed by potential cycling of the dummy cells between −1 to 1 V at a scan rate of 20 mV/s, followed by the EIS measurement.

2.3. DSSCs Cell Assembly and Characterization. The TiO_2 photoanode for DSSCs was prepared as follows: FTO glass (10 Ω/□, 3.1 mm thick, Nippon Sheet Glass) was immersed in 2% PK-LCG545 (Parker Corp.) at 50 °C for 30 min, and the surface was cleaned by sonication, followed by a deionized water rinse. The nano-TiO_2 paste (particle size 20 nm, product, Eternal) was then repeatedly screen-printed onto FTO glass until the film thickness was 6 μm. Finally, a 2 μm light scattering film (PST400, CCIC) was screen-printed onto the nano-TiO_2 film. The two-layer film was then sintered at 450 °C for 30 min in a furnace. Solutions of 40 mM and 10 mM $TiCl_4$ were applied in the pretreatment and post-treatment, respectively. Dye was impregnated by immersing the TiO_2 photoanode in a 0.2 mM YD2-o-C8 porphyrin solution (dye/CDCA ratio of 1:2 in tetrahydrofuran (THF)) at room temperature for 2 h. The effective area of the TiO_2 photoanode was 0.16 cm^2. The dye-adsorbed TiO_2 photoanode and the CEs (Pt and NG) were stacked face-to-face and were sealed with a 25 μm thick thermal-plastic Surlyn spacer (SX1170-25, Solaronix). A proper amount of liquid electrolyte (45 mM $Co(bpy)_3(TFSI)_3$ [where $(TFSI)_3$ = tris(2,2′-bipyridine)cobalt(III) bis(trifluoromethanesulfonimide)], 165 mM $Co(bpy)_3(TFSI)_2$, 100 mM lithium bis(trifluoromethane sulfonyl) imide (LiTFSI), 400 mM tri-*n*-butyl phosphate (TBP) in acetonitrile (AN)) was injected into the gap between the two electrodes. A black mask (6 × 6 mm^2) was used in the subsequent photovoltaic studies. The current−voltage (IV) curve for the DSSC cell was measured using a computer-controlled digital source meter (Keithley 2400) under exposure to a standard solar simulator (PEC-L01, Peccell) with 1 sun illumination (AM 1.5G, 100 $mW{\cdot}cm^{-2}$).

3. RESULTS AND DISCUSSION

We recently presented a low-cost solution-based process for the preparation of NG,[16] as shown in Figure 1, and investigated its electrocatalytic ability in I^-/I_3^- electrolyte. The relevant processing conditions are detailed in the Experimental Section. This method is different from previously reported methods in two ways.[17,18] First, the graphene nanosheets are synthesized using H_2SO_4/H_2O_2 as a mild oxidative agent to intercalate the graphite layers followed by microwave exfoliation, which produces fewer structural defects than the commonly used Hummers method using a strong oxidative agent (H_2SO_4/$KMnO_4$) and toxic chemical reduction ($NaBH_4$ or hydrazine). Second, cyanamide (NH_2CN) solution is used as an N-doping source and is mixed with the graphene suspension under ambient environment, which is more cost-effective and more readily scalable than the hydrothermal synthesis of graphene using NH_3 solution or freeze-drying a graphene hydrogel using a toxic NH_3 gas treatment.[19,20] Figure 2 shows the transmission electron microscopy (TEM) images for the graphene nanosheet and the NG. Figure 2b shows that curved type NGs are produced when an uneven stress/strain is generated between the intermediate cyanamide products (e.g., C_3N_4 polymer) and the graphene surfaces during the two-step annealing process.[21] The selective area electron diffraction (SAED) shown in Figure 2c is a typical carbon hexagonal diffraction pattern with stronger diffraction spots in the {0110} plane than in the{1120} plane, which demonstrates that the NG is a structure with few layers.[22,23] Figure 3a shows the X-ray photoelectron spectra (XPS) for NG, which has an obvious N 1s peak. The extra Na 1s peak may be attributable to the additive surfactant, sodium dodecyl sulfonate (SDS). The deconvoluted N 1s spectra in Figure 3b show only two peaks, centered at 398.2 and 401 eV, which are, respectively, assigned

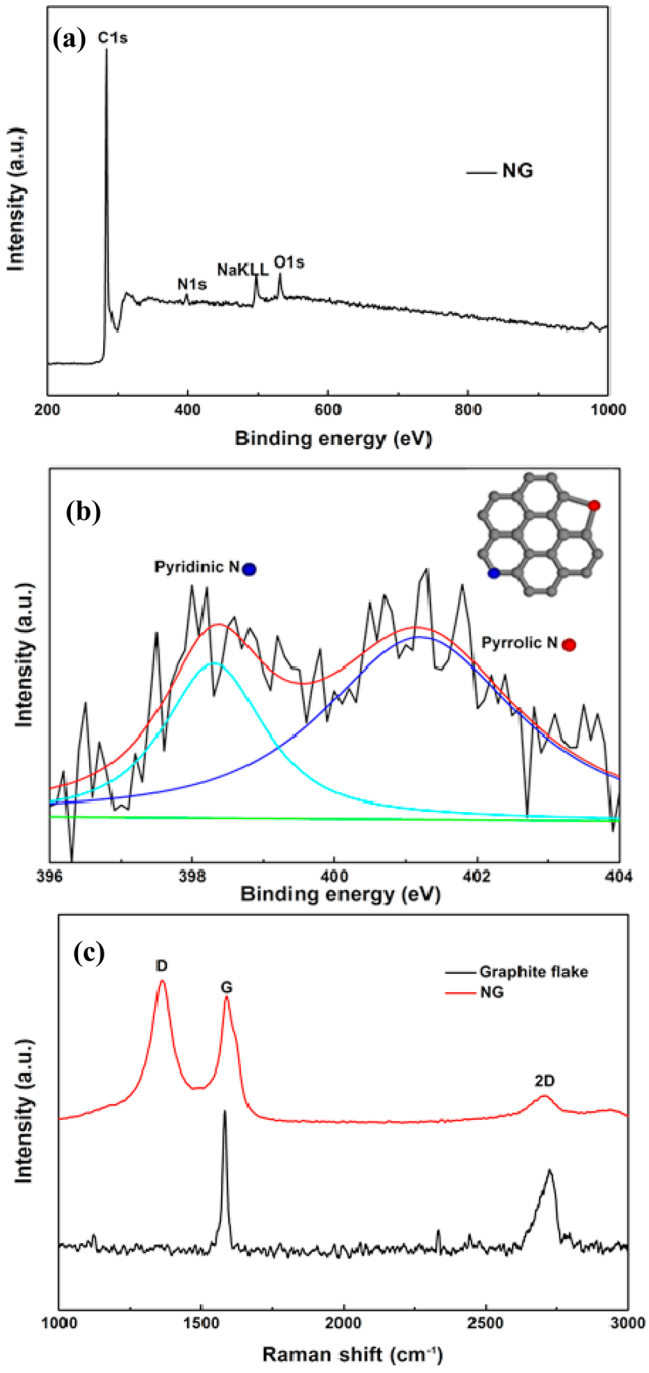

Figure 3. (a) The X-ray photoelectron spectra for NG; (b) the N 1s peak in the XPS spectra for NG and (c) the Raman spectra for NG and graphite flakes.

to the pyridinic and pyrrolic N structures. The pyridinic N is bonded to two carbon atoms and donates one p-electron to the aromatic π system. The pyrrolic N is incorporated into a five-membered heterocyclic ring, which is bonded to two carbon atoms and which contributes two p-electrons to the π system.[24] These two major structures of pyridinic/pyrrolic N improve the conductivity of the conjugated structure in the graphitic basal plane, and they provide lone pair electrons with a negative charge, which increases the electrocatalytic activity for the redox reaction, rather than other positively charged N-doping species, such as quaternary (~401 eV) and pyridine-N-oxide (~403 eV).[25,26] As noted, the preoxidation step plays an

DOI: 10.1021/am5083705
ACS Appl. Mater. Interfaces 2015, 7, 2116−2123

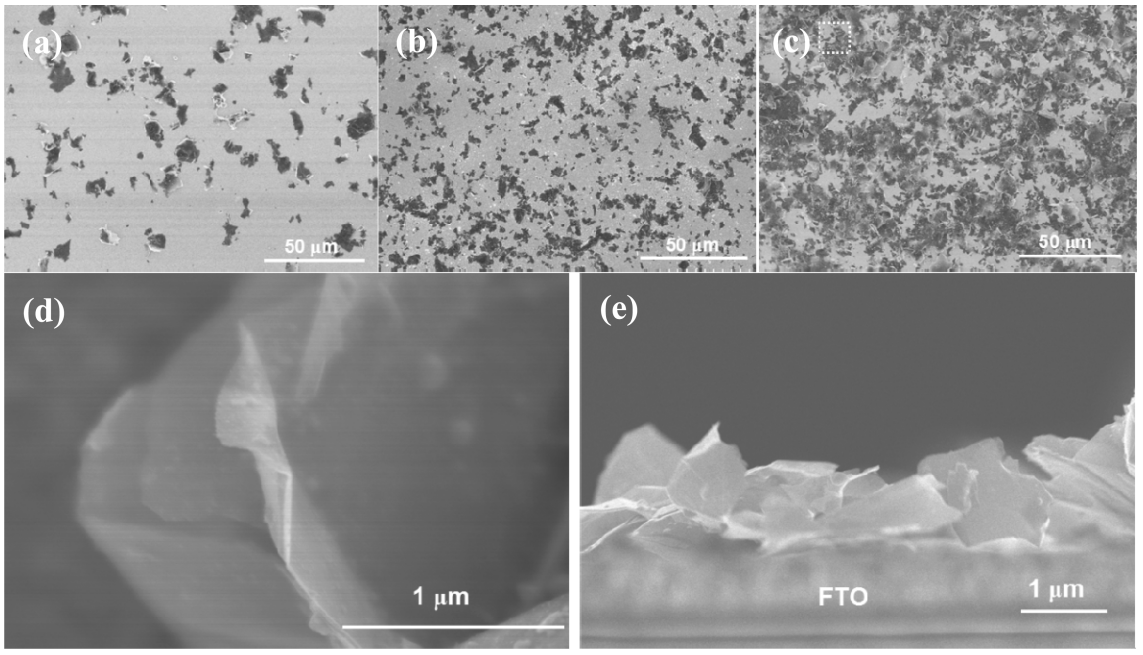

Figure 4. Field emission scanning electron microscope (FESEM) images of (a) NG1, (b) NG2, and (c) NG3 film on FTO. (d) A magnified image of the square region in c. (e) An image of a cross section of the NG3 film on FTO.

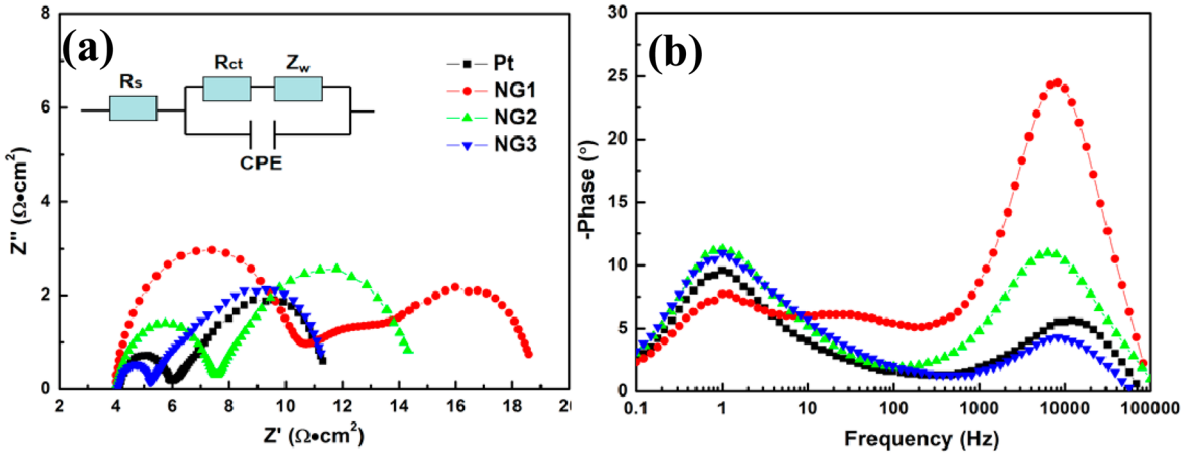

Figure 5. (a) The Nyquist plot for the symmetrical dummy cells for an NG CE and a Pt CE. The inset shows the equivalent circuit diagram for a thin film CE; (b) the Bode plot for an NG CE and a Pt CE.

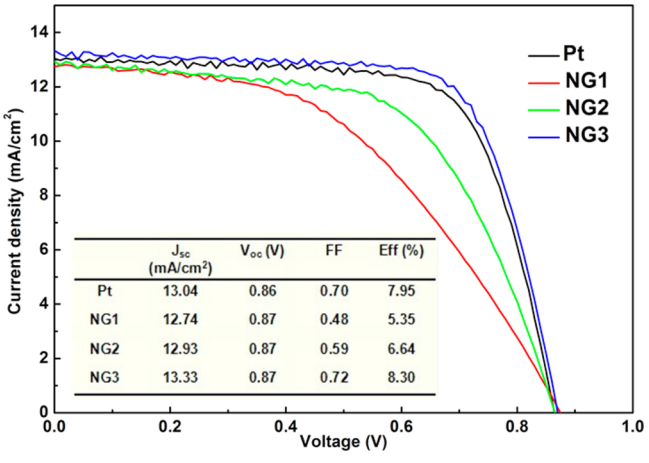

	J_{sc} (mA/cm²)	V_{oc} (V)	FF	Eff (%)
Pt	13.04	0.86	0.70	7.95
NG1	12.74	0.87	0.48	5.35
NG2	12.93	0.87	0.59	6.64
NG3	13.33	0.87	0.72	8.30

Figure 6. Current density−voltage characteristic for PSSCs with NG and Pt CEs.

important role in the incorporation of N into the graphene, since the N-sourced molecules preferentially react with oxygen functional groups. The Hummers method uses strong oxidizing and reduction agents to produce different oxygen functionalities, including C−O (285.2 eV), C−O−C (286.4 eV), and C═O (291.1 eV),[27] which leads to various N-doping types. In our case, the mild intercalation of H_2SO_4/H_2O_2 mainly causes C−O (285.6 eV) for the as-made graphene nanosheets, which are usually located within five- or six-membered rings at the edge of a graphene sheet. Therefore, the C−O groups react with the amine group of NH_2CN to principally form pyridinic and pyrrolic N structures. Thus, the synthesized NG should produce a superior redox reaction. In Figure S1 of the Supporting Information, the main peak at 284.5 eV corresponds to the graphitelike sp^2 C, which shows that most of the C atoms in the NG are arranged in a conjugated honeycomb lattice.[28] Raman spectroscopy was also used to determine the structural defects in the graphene-based material

DOI: 10.1021/am5083705
ACS Appl. Mater. Interfaces 2015, 7, 2116−2123

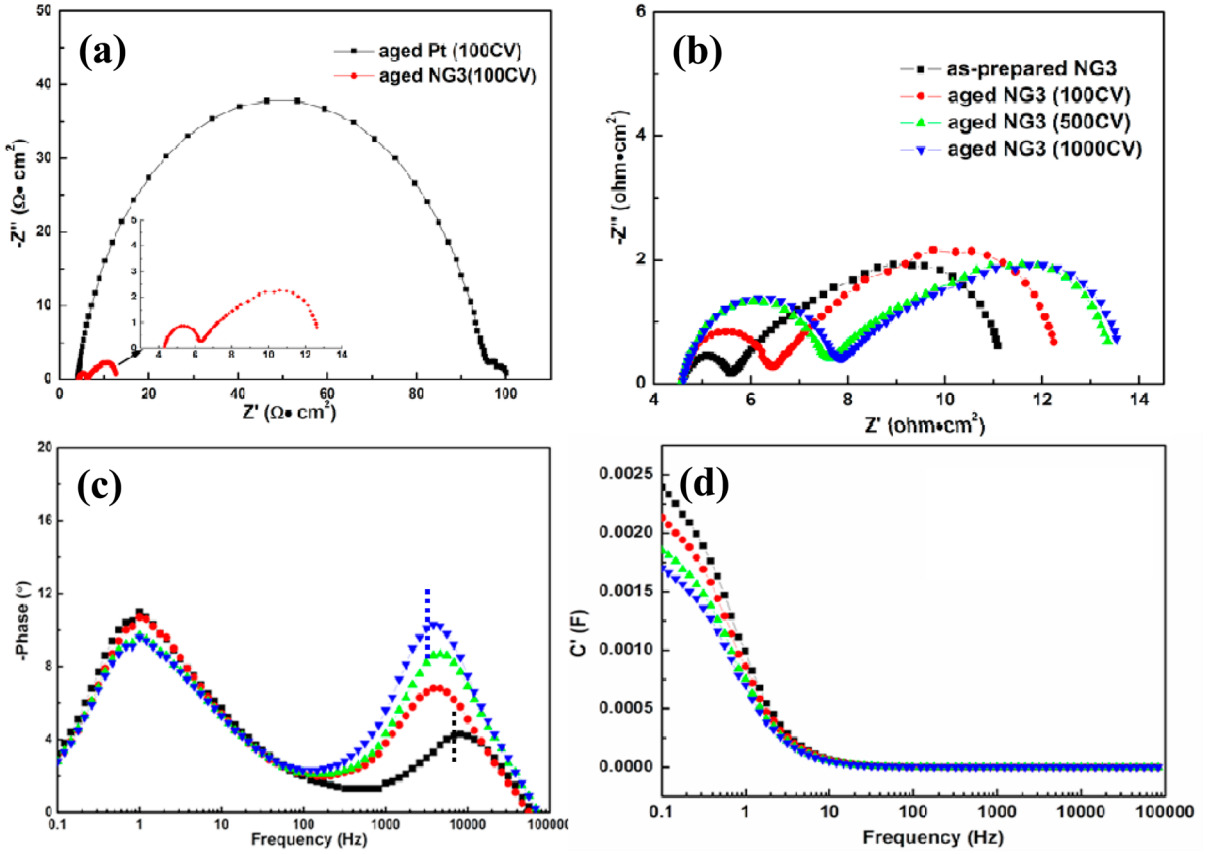

Figure 7. (a) The Nyquist plot for the symmetrical dummy cells for an NG3 CE and Pt CEs after 100 CV cycles at a scan rate of 20 mV/s. The inset shows a magnified image of an NG3. (b) The Nyquist plot for the symmetrical dummy cells for as-prepared NG3 (black) and aged NG3 after 100 cycles (red), 500 cycles (green), and 1000 cycles (blue). (c) The corresponding Bode plots for b. (d) The corresponding real-part capacitance vs frequency for b.

Table 1. EIS Results for the Symmetrical Dummy Cells for As-Prepared NG3 and Aged NG3

	R_s (Ω·cm^2)	R_{ct} (Ω·cm^2)	C' (mF) at 0.1 Hz
as-prepared NG3	1.98	0.45	2.39
aged NG3(100)	1.98	0.81	2.13
aged NG3(500)	1.98	1.10	1.85
aged NG3(1000)	1.98	1.38	1.70

on the D band (defect-related, breathing mode of A_{1g}) and the G band (the in-plane bond stretching motion of C sp^2 atoms, E_{2g} mode), as shown in Figure 3c. The NG exhibits a notably higher intensity ratio for the D and G band than the graphite flakes, which demonstrates that N-substitution induces structural distortion in the conjugated structure of graphene. Graphene with two layers and a few layers is known to have a broad and weak 2D band, which is the most prominent feature for the number layers of graphene in the Raman spectrum.[29] Here, a relatively broad and weak 2D band is seen at 2700 cm^{-1} for the NG sample, which demonstrates that an NG with a few layers was produced.

The NG nanosheets were redispersed in *N*-methyl pyrrolidone (NMP) and were then coated onto FTO glass by drop casting under three different conditions (NG1, 0.014; NG2, 0.028; and NG3, 0.056 mg/cm^2). The scanning electron microscopy (SEM) images are shown in Figure 4a–c. Figure 4d and e shows that the curved NG nanosheets allow more edge planes to be exposed to the electrolyte. The sharp atomic edges usually have more dangling bonds and N-doped active sites, which provide highly reactive unpaired electrons. To determine their electrocatalytic stability, the symmetrical dummy cells for NG and Pt were measured using EIS, and the results are shown in Figure 5a. The corresponding equivalent circuit diagram for the typical thin-film type CE is shown in the inset. The left semicircle in the higher frequency region relates to charge-transfer resistance (R_{ct}) and the corresponding constant phase element (CPE) at the electrode/electrolyte interface, and the right semicircle in the lower frequency region relates to the diffusion resistance of $[Co(bpy)_3]^{3+/2+}$ in the bulk electrolyte (Z_w).[30,31] It is seen that the electrocatalytic activity of NG is loading-dependent, and so NG3 has a lower value of R_{ct} (0.45 Ω·cm^2) than the other two NG CEs (NG1, 3.25 Ω·cm^2; NG2, 1.60 Ω·cm^2), even outperforming the Pt CE (0.77 Ω·cm^2). It is known that a shift to a lower characteristic frequency in the Bode plot indicates a slower charge transfer rate at the CE/electrolyte interface. The Bode plot shown in Figure 5b provides evidence that the position of the high-frequency peak (~10 000 Hz) for NG CEs is comparable to that for Pt CEs. Figure 6 shows the photocurrent density–voltage characteristic curves for PSSCs under simulated solar illumination (100 mW/cm^2, AM 1.5G). The Pt-based reference PSSC has a J_{sc} of 13.04 mA·cm^{-2}, a V_{oc} of 0.86 V, an FF of 0.70, and a PCE of 7.95%. The PSSC with an NG3 CE has an improved J_{sc} of 13.33 mA·cm^{-2} and a fill factor of 0.72, which gives a higher PCE of 8.30%. The PSSCs with NG1 and NG2 have poor values for fill factor (0.48, 0.59) and PCE (5.35%, 6.64%). These results are consistent with the EIS measurements. These findings

DOI: 10.1021/am5083705
ACS Appl. Mater. Interfaces 2015, 7, 2116–2123

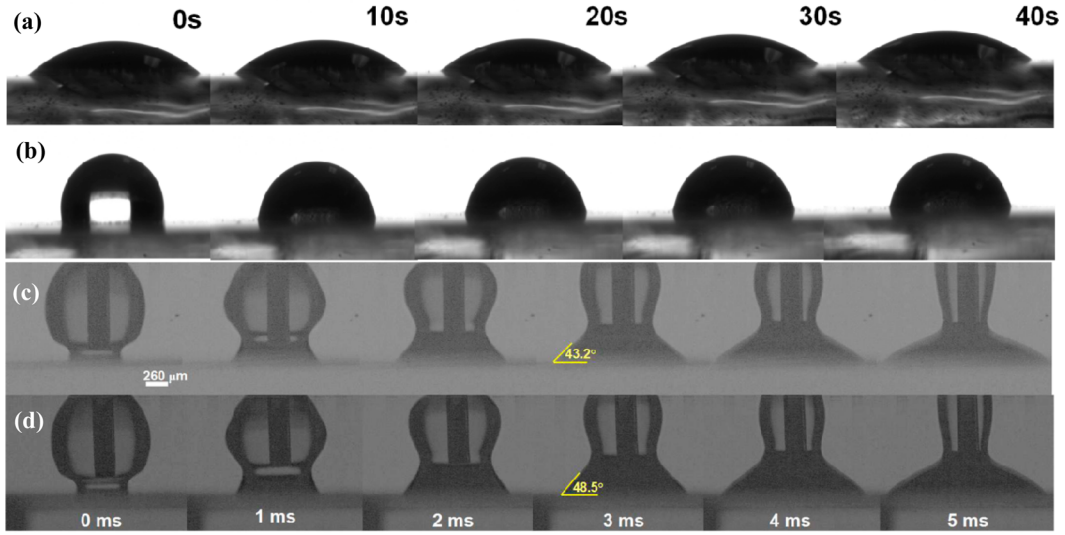

Figure 8. Dynamic process for DI water droplet permeation through (a) as-prepared NG3 film and (b) aged NG3 film (1000 cycles). Snapshots of cobalt electrolyte droplet permeation through (c) as-prepared NG3 film and (d) aged NG3 film (1000 cycles).

Table 2. Contact Angles for the As-Prepared and the Aged NG3 Films, Recorded Using a High-Speed Video Camera

	1 ms (deg)	2 ms (deg)	3 ms (deg)	4 ms (deg)	5 ms (deg)
as-prepared NG3	52.1	47.5	43.2	37.8	35.2
aged NG3(1000)	62.5	55.1	48.5	43.8	39.4

demonstrate that the PSSC with an NG3 CE outperforms that with a Pt CE because it has a higher electrocatalytic activity because of its lower value for R_{ct}. This clearly demonstrates the significant effect of using N-doped carbon-based CEs in PSSCs.

The NG3 and Pt symmetrical dummy cells were used for the catalytic stability test, and both were subjected to potential cycling between −1 to 1 V at a scan rate of 20 mV/s, followed by EIS measurements. The results are shown in Figure 7. A relatively slow scan rate was used in order to induce a harsh poisoning effect between the CEs and the $[Co(bpy)_3]^{3+/2+}$ in acetonitrile. Figure 7a shows that there is no noticeable change in the sheet resistance (R_s) in the high-frequency region, which means that the cycling potential has no significant effect on the value of R_s. The R_{ct} value for NG3 increases 2-fold, from 0.45 to 0.81 Ω·cm^2, after 100 potential cycles (denoted as aged NG3(100CV), and the R_{ct} value for the aged Pt increases 50-fold, from 0.77 to 45.54 Ω·cm^2. The improved electrocatalytic stability of NG indicates that it is eminently suitable for use in a $[Co(bpy)_3]^{3+/2+}$ mediator. The NG3 dummy cell was subsequently cycled another 900 times in a prolonged stability test. Figure 7b shows an approximately 3-fold increase in the value of R_{ct}, even after 1000 potential cycles, which demonstrates the high reliability of NG3 CE. The corresponding NG3 EIS data are summarized in Table 1. The Bode plot in Figure 7c shows that the position of the high-frequency peak shifts to a lower value after 1000 cycles, which means a slower charge transfer rate at the CE/electrolyte interface because of the poisoning effect.[32] Figure 7d shows the variation in the real-part capacitance (C') with the frequency. For the same specific surface area and film morphology, the aged NG3 exhibits a smaller capacitance than the as-prepared NG3 in the low-frequency region (~0.1 Hz), which indicates that the electrode/electrolyte interfacial contact becomes worse.[33] This finding suggests that the wettability of the NG surface and its relationship with $[Co(bpy)_3]^{3+/2+}$ ions is worthy of study. In general, pristine graphene is intrinsically hydrophobic. N-Substitution in the graphene lattice not only tailors the electronic structure of the graphene but also renders it more wettable.[34] A previous work by the authors showed that the dewettability of the NG surface is influenced by airborne contamination of hydrocarbons. Therefore, to avoid air contact, the aged NG3(1000CV) CEs in the dummy cell were disassembled after the EIS test and were rinsed using copious amounts of DI water, followed by immediate drying in a vacuum oven at 70 °C for 4 h. A pronounced difference in the wettability is seen in Figure 8a and b when DI water is used as a probing liquid. The as-prepared NG3 is hydrophilic (~40.5°), but the aged NG3(1000CV) is hydrophobic (~108.5°). Because the viscosity of DI water (1 cP at 20 °C) is much higher than that of acetonitrile-based electrolyte (0.35 cP), the dynamic wetting behavior at the interface between the NG and the $[Co(bpy)_3]^{3+/2+}$ electrolyte were recorded using a high-speed video camera (2000 fps), and the results are shown in Videos S1 and S2 of the Supporting Information. The captured images in Figures 8c and d show that the aged NG3 is less wettable than as-prepared NG3 at every millisecond, as listed in Table 2 (e.g., aged NG3, 48.5°, and as-prepared NG3, 43.2°, at 3 ms). This demonstrates that some of the active sites of the NG3 are passivated, which produces a less-wettable surface and poor electrocatalytic performance. Future research will be needed to improve N-doping carbon-based nanomaterials and Co-based redox complexes so that the nondegradable electrocatalytic performance for PSSC can be achieved.

4. CONCLUSION

Nitrogen-doped graphene nanosheets were prepared using a low-cost solution-based process and were used as a Pt-free CE for the reduction of $[Co(bpy)_3]^{3+/2+}$ in porphyrin-sensitized solar cells. The XPS evidence shows that the mild intercalation of H_2SO_4/H_2O_2 primarily causes C−O (285.6 eV), which is usually located within five- or six-membered rings at the edge of a graphene sheet. Therefore, C−O groups react with NH_2CN to principally form negatively charged pyridinic/pyrrolic N

DOI: 10.1021/am5083705
ACS Appl. Mater. Interfaces 2015, 7, 2116−2123

structures, which effectively increases the electrocatalytic activity in the redox reaction. The NG3 CE exhibits a lower value of R_{ct} for the $[Co(bpy)_3]^{3+/2+}$ redox couple and a significantly better electrochemical stability during prolonged potential cycles than those for the Pt CE. The PSSC-NG3 CE outperforms the PSSC-Pt CE because it has greater FF and J_{sc} values. It is also proved that the poisoning effect of the $[Co(bpy)_3]^{3+/2+}$ mediator is correlated with the degradation of active sites and surface wettability of NG3 CEs, which affects the charge-transfer process. These results suggest that NG is eminently suitable as a low-cost Pt-free CE in conjunction with a $[Co(bpy)_3]^{3+/2+}$ based electrolyte to achieve the reliable high-performance PSSCs.

■ ASSOCIATED CONTENT

Supporting Information

Additional information details about X-ray photoelectron spectroscopy (XPS) images of graphene and NG nanosheets. This material is available free of charge via the Internet at http://pubs.acs.org/.

■ AUTHOR INFORMATION

Corresponding Authors

*Tel: (852) 2859 2639. Fax: (852) 2858 5415. E-mail: hpfeng@hku.hk (S.P.F.).

*Tel: (886) 3571 5131. Fax: (886) 3571 5408. E-mail: tcwei@mx.nthu.edu.tw (T.C.W.).

Notes

The authors declare no competing financial interest.

■ ACKNOWLEDGMENTS

The authors thank Dr. A. H. C. Shum and Mr. Zhou Liu in the University of Hong Kong for their assistance in the use of the high-speed video camera. This work was supported by the General Research Fund of the Research Grants Council of Hong Kong Special Administrative Region, China: Award Number: HKU 712213E (S.P.Feng).

■ REFERENCES

(1) Chen, C.-Y.; Wang, M.; Li, J.-Y.; Pootrakulchote, N.; Alibabaei, L.; Ngoc-le, C.-h.; Decoppet, J.-D.; Tsai, J.-H.; Grätzel, C.; Wu, C.-G. Highly efficient light-harvesting ruthenium sensitizer for thin-film dye-sensitized solar cells. *ACS Nano* **2009**, *3*, 3103−3109.

(2) Boschloo, G.; Hagfeldt, A. Characteristics of the iodide/triiodide redox mediator in dye-sensitized solar cells. *Acc. Chem. Res.* **2009**, *42*, 1819−1826.

(3) O'Regan, B. C.; Walley, K.; Juozapavicius, M.; Anderson, A.; Matar, F.; Ghaddar, T.; Zakeeruddin, S. M.; Klein, C.; Durrant, J. R. Structure/function relationships in dyes for solar energy conversion: a two-atom change in dye structure and the mechanism for its effect on cell voltage. *J. Am. Chem. Soc.* **2009**, *131*, 3541−3548.

(4) Yella, A.; Lee, H. W.; Tsao, H. N.; Yi, C.; Chandiran, A. K.; Nazeeruddin, M. K.; Diau, E. W.; Yeh, C. Y.; Zakeeruddin, S. M.; Grätzel, M. Porphyrin-sensitized solar cells with cobalt (II/III)-based redox electrolyte exceed 12% efficiency. *Science* **2011**, *334*, 629−34.

(5) Feldt, S. M.; Gibson, E. A.; Gabrielsson, E.; Sun, L.; Boschloo, G.; Hagfeldt, A. Design of organic dyes and cobalt polypyridine redox mediators for high-efficiency dye-sensitized solar cells. *J. Am. Chem. Soc.* **2010**, *132*, 16714−16724.

(6) Yum, J.-H.; Baranoff, E.; Kessler, F.; Moehl, T.; Ahmad, S.; Bessho, T.; Marchioro, A.; Ghadiri, E.; Moser, J.-E.; Yi, C. A cobalt complex redox shuttle for dye-sensitized solar cells with high open-circuit potentials. *Nat. Commun.* **2012**, *3*, 631.

(7) Zhai, P.; Chang, Y.-H.; Huang, Y.-T.; Wei, T.-C.; Su, H.; Feng, S.-P. Water-soluble Microwave-exfoliated Graphene Nanosheet/Platinum Nanoparticle Composite and Its Application in Dye-Sensitized Solar Cells. *Electrochim. Acta* **2014**, *132*, 186−192.

(8) Kavan, L.; Yum, J.-H.; Grätzel, M. Graphene nanoplatelets outperforming platinum as the electrocatalyst in co-bipyridine-mediated dye-sensitized solar cells. *Nano Lett.* **2011**, *11*, 5501−5506.

(9) Kavan, L.; Yum, J.-H.; Grätzel, M. Optically transparent cathode for Co (III/II) mediated dye-sensitized solar cells based on graphene oxide. *ACS Appl. Mater. Interfaces* **2012**, *4*, 6999−7006.

(10) Kavan, L.; Yum, J.-H.; Nazeeruddin, M. K.; Grätzel, M. Graphene nanoplatelet cathode for Co (III)/(II) mediated dye-sensitized solar cells. *ACS Nano* **2011**, *5*, 9171−9178.

(11) Ju, M. J.; Kim, J. C.; Choi, H.-J.; Choi, I. T.; Kim, S. G.; Lim, K.; Ko, J.; Lee, J.-J.; Jeon, I.-Y.; Baek, J.-B. N-Doped Graphene Nanoplatelets as Superior Metal-Free Counter Electrodes for Organic Dye-Sensitized Solar Cells. *ACS Nano* **2013**, *7*, 5243−5250.

(12) Ju, M. J.; Jeon, I. Y.; Kim, J. C.; Lim, K.; Choi, H. J.; Jung, S. M.; Choi, I. T.; Eom, Y. K.; Kwon, Y. J.; Ko, J. Graphene Nanoplatelets Doped with N at its Edges as Metal-Free Cathodes for Organic Dye-Sensitized Solar Cells. *Adv. Mater.* **2014**, *26*, 3055−3062.

(13) Ju, M. J.; Jeon, I.-Y.; Lim, K.; Kim, J. C.; Choi, H.-J.; Choi, I. T.; Eom, Y. K.; Kwon, Y. J.; Ko, J.; Lee, J.-J. Edge-carboxylated graphene nanoplatelets as oxygen-rich metal-free cathodes for organic dye-sensitized solar cells. *Energy Environ. Sci.* **2014**, *7*, 1044−1052.

(14) Hou, S.; Cai, X.; Wu, H.; Yu, X.; Peng, M.; Yan, K.; Zou, D. Nitrogen-doped graphene for dye-sensitized solar cells and the role of nitrogen states in triiodide reduction. *Energy Environ. Sci.* **2013**, *6*, 3356−3362.

(15) Jeong, H. M.; Lee, J. W.; Shin, W. H.; Choi, Y. J.; Shin, H. J.; Kang, J. K.; Choi, J. W. Nitrogen-doped graphene for high-performance ultracapacitors and the importance of nitrogen-doped sites at basal planes. *Nano Lett.* **2011**, *11*, 2472−2477.

(16) Zhai, P.; Wei, T. C.; Chang, Y. H.; Huang, Y. T.; Yeh, W. T.; Su, H.; Feng, S. P. High Electrocatalytic and Wettable Nitrogen-Doped Microwave-Exfoliated Graphene Nanosheets as Counter Electrode for Dye-Sensitized Solar Cells. *Small* **2014**, *10*, 3347−3353.

(17) Gao, X.; Jang, J.; Nagase, S. Hydrazine and thermal reduction of graphene oxide: reaction mechanisms, product structures, and reaction design. *J. Phys. Chem. C* **2009**, *114*, 832−842.

(18) Park, S.; An, J.; Potts, J. R.; Velamakanni, A.; Murali, S.; Ruoff, R. S. Hydrazine-reduction of graphite-and graphene oxide. *Carbon* **2011**, *49*, 3019−3023.

(19) Yen, M.-Y.; Hsieh, C.-K.; Teng, C.-C.; Hsiao, M.-C.; Liu, P.-I.; Ma, C.-C. M.; Tsai, M.-C.; Tsai, C.-H.; Lin, Y.-R.; Chou, T.-Y. Metal-free, nitrogen-doped graphene used as a novel catalyst for dye-sensitized solar cell counter electrodes. *RSC Adv.* **2012**, *2*, 2725−2728.

(20) Xue, Y.; Liu, J.; Chen, H.; Wang, R.; Li, D.; Qu, J.; Dai, L. Nitrogen-Doped Graphene Foams as Metal-Free Counter Electrodes in High-Performance Dye-Sensitized Solar Cells. *Angew. Chem., Int. Ed.* **2012**, *51*, 12124−12127.

(21) Wen, Z.; Wang, X.; Mao, S.; Bo, Z.; Kim, H.; Cui, S.; Lu, G.; Feng, X.; Chen, J. Crumpled Nitrogen-Doped Graphene Nanosheets with Ultrahigh Pore Volume for High-Performance Supercapacitor. *Adv. Mater.* **2012**, *24*, 5610−5616.

(22) Gu, W.; Zhang, W.; Li, X.; Zhu, H.; Wei, J.; Li, Z.; Shu, Q.; Wang, C.; Wang, K.; Shen, W. Graphene sheets from worm-like exfoliated graphite. *J. Mater. Chem.* **2009**, *19*, 3367−3369.

(23) Lotya, M.; Hernandez, Y.; King, P. J.; Smith, R. J.; Nicolosi, V.; Karlsson, L. S.; Blighe, F. M.; De, S.; Wang, Z.; McGovern, I. Liquid phase production of graphene by exfoliation of graphite in surfactant/water solutions. *J. Am. Chem. Soc.* **2009**, *131*, 3611−3620.

(24) Lai, L.; Potts, J. R.; Zhan, D.; Wang, L.; Poh, C. K.; Tang, C.; Gong, H.; Shen, Z.; Lin, J.; Ruoff, R. S. Exploration of the active center structure of nitrogen-doped graphene-based catalysts for oxygen reduction reaction. *Energy Environ. Sci.* **2012**, *5*, 7936−7942.

(25) Xu, B.; Hou, S.; Cao, G.; Wu, F.; Yang, Y. Sustainable nitrogen-doped porous carbon with high surface areas prepared from gelatin for supercapacitors. *J. Mater. Chem.* **2012**, *22*, 19088−19093.

(26) Hulicova-Jurcakova, D.; Kodama, M.; Shiraishi, S.; Hatori, H.; Zhu, Z. H.; Lu, G. Q. Nitrogen-Enriched Nonporous Carbon

DOI: 10.1021/am5083705
ACS Appl. Mater. Interfaces 2015, 7, 2116−2123

Electrodes with Extraordinary Supercapacitance. *Adv. Funct. Mater.* **2009**, *19*, 1800−1809.
(27) Wang, G.; Xing, W.; Zhuo, S. Nitrogen-doped graphene as low-cost counter electrode for high-efficiency dye-sensitized solar cells. *Electrochim. Acta* **2013**, *92*, 269−275.
(28) Wei, D.; Liu, Y.; Wang, Y.; Zhang, H.; Huang, L.; Yu, G. Synthesis of N-doped graphene by chemical vapor deposition and its electrical properties. *Nano Lett.* **2009**, *9*, 1752−1758.
(29) Graf, D.; Molitor, F.; Ensslin, K.; Stampfer, C.; Jungen, A.; Hierold, C.; Wirtz, L. Spatially resolved Raman spectroscopy of single- and few-layer graphene. *Nano Lett.* **2007**, *7*, 238−242.
(30) Roy-Mayhew, J. D.; Bozym, D. J.; Punckt, C.; Aksay, I. A. Functionalized graphene as a catalytic counter electrode in dye-sensitized solar cells. *ACS Nano* **2010**, *4*, 6203−6211.
(31) Gong, F.; Li, Z.; Wang, H.; Wang, Z.-S. Enhanced electrocatalytic performance of graphene via incorporation of SiO_2 nanoparticles for dye-sensitized solar cells. *J. Mater. Chem.* **2012**, *22*, 17321−17327.
(32) Jeong, H.; Pak, Y.; Hwang, Y.; Song, H.; Lee, K. H.; Ko, H. C.; Jung, G. Y. Enhancing the Charge Transfer of the Counter Electrode in Dye-Sensitized Solar Cells Using Periodically Aligned Platinum Nanocups. *Small* **2012**, *8*, 3757−3761.
(33) Toupin, M.; Bélanger, D.; Hill, I. R.; Quinn, D. Performance of experimental carbon blacks in aqueous supercapacitors. *J. Power Sources* **2005**, *140*, 203−210.
(34) Ostrowski, J. H.; Eaves, J. D. The Tunable Hydrophobic Effect on Electrically Doped Graphene. *J. Phys. Chem. B* **2014**, *118*, 530−536.

DOI: 10.1021/am5083705
ACS Appl. Mater. Interfaces 2015, 7, 2116−2123